

Benzene Hydroxylation by Bioinspired Copper(II) Complexes: Coordination Geometry versus Reactivity

Sethuraman Muthuramalingam, Karunanithi Anandababu, Marappan Velusamy, and Ramasamy Mayilmurugan*

Cite This: <https://dx.doi.org/10.1021/acs.inorgchem.9b03676>

Read Online

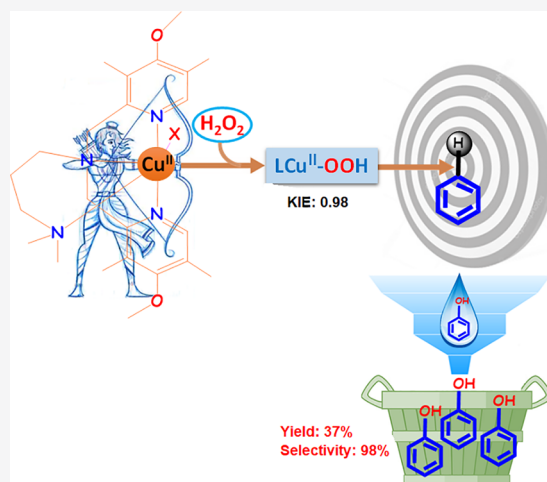
ACCESS |

Metrics & More

Article Recommendations

Supporting Information

ABSTRACT: A series of bioinspired copper(II) complexes of N_4 -tripodal and sterically crowded diazepane-based ligands have been investigated as catalysts for functionalization of the aromatic C–H bond. The tripodal-ligand-based complexes exhibited distorted trigonal-bipyramidal (TBP) geometry (τ , 0.70) around the copper(II) center; however, diazepane-ligand-based complexes adopted square-pyramidal (SP) geometry (τ , 0.037). The Cu– N_{py} bonds (2.003–2.096 Å) are almost identical and shorter than Cu– N_{amine} bonds (2.01–2.148 Å). Also, their Cu–O (Cu– O_{water} , 1.988 Å; Cu– $O_{triflate}$, 2.33 Å) bond distances are slightly varied. All of the complexes exhibited $Cu^{2+} \rightarrow Cu^+$ redox couples in acetonitrile, where the redox potentials of TBP-based complexes (–0.251 to –0.383 V) are higher than those of SP-based complexes (–0.450 to –0.527 V). The d–d bands around 582–757 nm and axial patterns of electron paramagnetic resonance spectra [$g_{||}$, 2.200–2.251; $A_{||}$, $(146–166) \times 10^{-4} \text{ cm}^{-1}$] of the complexes suggest the existence of five-coordination geometry. The bonding parameters showed $K_{||} > K_{\perp}$ for all complexes, corresponding to out-of-plane π bonding. The complexes catalyzed direct hydroxylation of benzene using 30% H_2O_2 and afforded phenol exclusively. The complexes with TBP geometry exhibited the highest amount of phenol formation (37%) with selectivity (98%) superior to that of diazepane-based complexes (29%), which preferred to adopt SP-based geometry. Hydroxylation of benzene likely proceeded via a Cu^{II} -OOH key intermediate, and its formation has been established by electrospray ionization mass spectrometry, vibrational, and electronic spectra. Their formation constants have been calculated as $(2.54–11.85) \times 10^{-2} \text{ s}^{-1}$ from the appearance of an O (π^*) \rightarrow Cu ligand-to-metal charge-transfer transition around 370–390 nm. The kinetic isotope effect (KIE) experiments showed values of 0.97–1.12 for all complexes, which further supports the crucial role of Cu-OOH in catalysis. The ^{18}O -labeling studies using $H_2^{18}O_2$ showed a 92% incorporation of ^{18}O into phenol, which confirms H_2O_2 as the key oxygen supplier. Overall, the coordination geometry of the complexes strongly influenced the catalytic efficiencies. The geometry of one of the Cu^{II} -OOH intermediates has been optimized by the density functional theory method, and its calculated electronic and vibrational spectra are almost similar to the experimentally observed values.



INTRODUCTION

Phenol is an industrially valuable precursor material used to synthesize several chemical products.^{1–3} Currently, it is manufactured only by a three-step cumene process from benzene and dioxygen (O_2) as oxidants, where the overall yield of phenol is ~5%.^{4–6} Phenol is also produced by the sulfonation^{6a} and Dow^{6b} processes. The main disadvantages of these processes are poor atom economy and high reaction temperature and pressure. Right now, the Dow process is no longer under practice because of its adverse chlorine economy and alkali production. Therefore, it is extremely essential to adopt suitable methods for the industrial manufacture of phenol, which should preferably defeat the shortcomings of the cumene process.^{4–6} Therefore, direct benzene hydroxylation is one of the most efficient ways to produce phenol with a better

atom economy. This process mostly occurs via the activation of one of the C–H bonds; however, its higher bond energy (460 kJ mol^{-1}) makes that difficult.^{7–9} In recent years, many researchers are thoughtfully exploring the possibility of an efficient methodology by designing new catalysts that are able to perform selective phenol synthesis in a single step from benzene and greener oxidants like O_2 ¹⁰ or activated oxygen sources.¹¹ The efforts through conventional approaches like

Received: December 18, 2019

electrochemical oxidation,^{12a} photochemical oxidation,^{12b} and Fenton-type reaction^{12c} are reported to afford lower yields of phenol with poor selectivity. On the other hand, heterogeneous catalysts were also employed to produce phenol using H₂O₂,^{13–15} wherein leaching caused low catalytic efficiency and product loss. Hence, bioinspired transition-metal-based homogeneous catalysts may offer better advantages and can perform catalysis under mild conditions. The efficiency of these catalysts can be regulated by changing the ligand electronics and thus redox potentials.¹⁶

In nature, copper monooxygenases such as dopamine β -monooxygenase, tyramine β -monooxygenase, peptidylglycine- α -hydroxylating monooxygenase, polysaccharide monooxygenases,^{17–21} methane monooxygenase,^{22,23} and tyrosinase²⁴ are well-known for activating challenging C–H bonds elegantly at ambient condition using O₂. Over the past few decades, bioinorganic chemists successfully reported numerous bioinspired model complexes to activate the C–H bond. Itoh and co-workers reported several model copper(II) complexes for quantitative intramolecular hydroxylation at the benzylic position.²⁵ Karlin and co-workers showed intramolecular hydroxylation on electron-rich aromatic systems using bioinspired models of tyrosinase, where various copper complexes and their reactive intermediates were extensively studied.²⁶ All of these intramolecular C–H functionalizations are stoichiometric and are known to occur via copper superoxide species.^{25,26} Recently, Gagnon and Tolman have shown [CuOH]²⁺ as the reactive core to activate the C–H bond of polysaccharide using Cu^{III}-OH complexes of pyridinedicarboxamide-based ligands under stoichiometric condition.²⁷

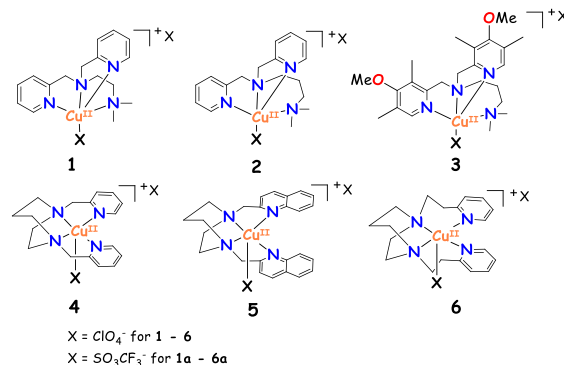
On the other hand, in 2011, Perez and co-workers reported [Tp^xCu(NCMe)] (Tp^x = hydrotrispyrazolylborate ligand) as a catalyst for benzene hydroxylation and attained a phenol yield of 21% but with poor selectivity (phenol:benzoquinone = 70:30) at 80 °C.²⁸ Later in 2017, the same group proposed two possible mechanisms, such as electrophilic aromatic substitution via copper oxyl species and a rebound mechanism by experimental and density functional theory (DFT) studies.²⁹ In 2015, Kodera and co-workers showed benzene hydroxylation using a dicopper(II) complex of the hpa ligand [Cu₂(μ -OH)6-hpa]³⁺, where hpa is 1,2-bis[2-[bis(2-pyridylmethyl)aminomethyl]-6-pyridyl]ethane. It afforded 22% of phenol conversion and 4.8% of *p*-benzoquinone over 40 h.³⁰ Liu and co-workers reported the catalyst [CuL(HOCH₃)ClO₄]⁺ (L = 2-[[[(1-methyl-1*H*-imidazol-2-yl)methyl](pyridin-2-ylmethyl)amino]methyl]-2-*tert*-butylphenol) for benzene hydroxylation and displayed a yield of 14.6% phenol with a turnover number (TON) of 48.7 at 80 °C.³¹ Therefore, the strategy and synthesis of bioinspired catalysts for benzene hydroxylation remain a challenging and evergreen interest to date. This article reports bioinspired copper(II) complexes of N₄-tripodal and sterically constrained diazepane-based ligands, which adopted distorted trigonal-bipyramidal (TBP)- and square-pyramidal (SP)-based geometries around copper centers, respectively. The complexes have been employed as catalysts for benzene hydroxylation to produce phenol by utilizing the H₂O₂ oxygen source. The TBP-based complexes exhibited selective phenol formation yields of up to 37% at 60 °C and 16% at 25 °C, which are relatively higher than those of SP-based complexes and other reported copper complexes.^{28–31} These are novel examples of Cu^{II}-N₄ complexes that illustrate the importance of coordination geometry versus catalytic

efficiency and selectivity. The present tripodal ligand designs and their electronics provide noteworthy variances from sterically constrained diazepane-based ligands and other previously reported copper(II) complexes and thus enhanced catalytic performances.

RESULTS AND DISCUSSION

Synthesis and Characterization of Complexes. The ligands *N,N*-bis(2-pyridylmethyl)-*N',N'*-dimethylethane-1,2-diamine (L1), *N,N*-bis(2-pyridylmethyl)-*N',N'*-dimethylpropane-1,3-diamine (L2), *N,N*-bis(4-methoxy-3,5-dimethylpyridin-2-ylmethyl)-*N',N'*-dimethylpropane-1,3-diamine (L3), 1,4-bis(2-pyridinylmethyl)-1,4-diazepane (L4), 1,4-bis(2-quinolylmethyl)-1,4-diazepane (L5), and 1,4-bis(2-pyridinylethyl)-1,4-diazepane (L6) were synthesized as reported previously by us.^{32–34} The copper(II) complexes [Cu(L)(ClO₄)]ClO₄ (1–6) have been isolated by the reactions of Cu(ClO₄)₂·6H₂O and the respective tetradentate N₄ ligands in methanol (Scheme 1).³⁵ Additionally, SO₃CF₃[−]-ion-containing com-

Scheme 1. Structures of Copper(II) Complexes 1–6



plexes [Cu(L)(SO₃CF₃)]SO₃CF₃ (1a–6a) were also synthesized to understand the influence of counterions in catalysis. The complexes have been characterized by various analytical methods (cf. below). Complexes 4 and 6 were crystallized, and their molecular structures were reported as distorted SP geometry.³⁵ Suitable single crystals of 2a and 4a were isolated by diethyl ether diffusion into complexes in acetonitrile (CH₃CN) and used for X-ray diffraction studies.

Molecular Structures of Copper(II) Complexes. Single crystals of 2a have been crystallized as [Cu(L)(H₂O)](SO₃CF₃)₂ in a monoclinic P21/c space group (Figure 1 and

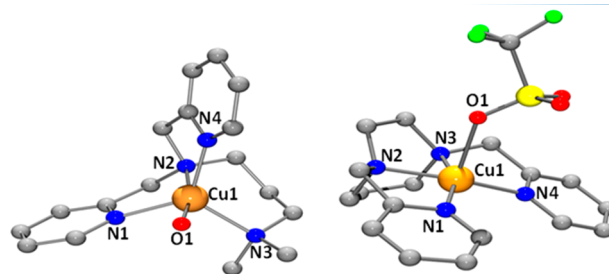


Figure 1. Molecular structures of [Cu(L2)(H₂O)](CF₃SO₃)₂ (2a) and [Cu(L4)(CF₃SO₃)](CF₃SO₃) (4a). Thermal ellipsoids are drawn from 50% probability. Hydrogen atoms and CF₃SO₃[−] at the outer coordination are excluded for lucidness.

Tables 1 and S6). It adopted a five-coordinate distorted TBP geometry. The distortion is predicted by the Addison

Table 1. Bond Distances^a (Å) and Bond Angles^a (deg)

	2a	4a
Cu(1)–N(1)	2.096(5)	2.003(3)
Cu(1)–N(2)	2.033(5)	2.01(8)
Cu(1)–N(3)	2.148(5)	2.02(4)
Cu(1)–N(4)	2.084(5)	2.015(17)
Cu(1)–O(1)	1.998(5)	2.33(5)
N(1)–Cu(1)–N(2)	81.05(18)	83.5(5)
N(1)–Cu(1)–N(4)	113.74(19)	116.6(7)
N(2)–Cu(1)–N(4)	80.51(19)	158.87(18)
N(1)–Cu(1)–N(3)	125.2(2)	161.11(10)
N(2)–Cu(1)–N(3)	96.3(2)	79.2(16)
N(4)–Cu(1)–N(3)	119.3(2)	83.6(17)
N(1)–Cu(1)–O(1)	94.7(2)	91.63(3)
N(2)–Cu(1)–O(1)	167.2(2)	91(3)
N(4)–Cu(1)–O(1)	92.3(2)	103(3)
N(3)–Cu(1)–O(1)	96.5(2)	95.8(14)

^aStandard deviations in parentheses.

parameter $\tau = 0.70$ [$\tau = (\beta - \alpha)/60$; $\beta = 167.2^\circ$ and $\alpha = 125.2^\circ$], which is 0 and 1 for the SP and TBP geometries, respectively.³⁶ The TBP geometry is constituted by nitrogen atoms of the ligand L2 and one H₂O molecule at axial coordination. The observed Cu–N (2.033–2.148 Å) and Cu–O_{water} (1.998 Å) bond lengths are analogous to the previously reported copper(II) complexes with TBP geometry.³⁷ One nitrogen atom [N(2)] and H₂O molecule [O(1)] occupied the axial sites with a N(2)–Cu–O(1) bond angle of 167.2(2)°, which is higher than the bond angle N(1)–Cu–N(3) [125.2(2)°] at the equatorial site and the bond angle N(4)–Cu–N(3) [119.3(2)°] constituted by pyridine nitrogen donors. The distortion in the TBP geometry is revealed by variation of the N(1)–Cu–N(3) [125.2(2)°], N(3)–Cu–N(4) [119.3(2)°], and N(1)–Cu–N(4) [113.74(19)°] bond angles at the equatorial site. The axial bond angle N(2)–Cu–O(1) deviated from 180°, which additionally confirmed the existence of significant distortion in the coordination geometry.³⁵ The complexes of the other tripodal ligands L1 and L3 are expected to display similar TBP-based coordination geometries.

The molecular structure of 4a exhibited the Cu–N₄O coordination sphere (Figure 1) with a more SP geometry, which is revealed from the τ value of 0.037 (Table 1). The four nitrogen atoms of L4 occupied equatorial locations, whereas an oxygen atom of the CF₃SO₃[−] ion was placed at the axial position. The observed Cu–O_{triflate} bond distance of 4a [2.33(5) Å] is lengthier than the Cu–O_{water} bond length of 2a but shorter than those of 4 [2.46(2) Å] and 6 [2.52(6) Å], which adopted identical distorted SP geometries.³⁵ This axial elongation of Cu–O_{triflate} is possibly caused by the pseudo-Jahn–Teller effect and positioned to be highly labile. This can be easily replaced by a solvent molecule or H₂O₂ during catalysis. The bond lengths Cu–N_{py} (2.00 and 2.01 Å) and Cu–N_{amine} (2.01 and 2.02 Å) of 4a are indistinguishable from those of 2a but somewhat lower than those of 4 (Cu–N_{py}, 1.95 and 1.99 Å; Cu–N_{amine}, 1.98 and 2.01 Å) and 6 (Cu–N_{py}, 2.01 and 2.02 Å; Cu–N_{amine}, 2.03 and 2.032 Å).³⁵ The N(1)–Cu–N(3) [161.11(10)°] and N(2)–Cu–N(4) [158.87(18)°]

bond angles of 4a are lower than those expected for normal SP geometry. The other bond angles O(1)–Cu–N(1) [91.63(3)°], O(1)–Cu–N(2) [91(3)°], N(4)–Cu–O(1) [103(3)°], and N(3)–Cu–O(1) [95.8(14)°] are larger than the value expected for normal SP geometry (90°); however, the N(1)–Cu–N(2) [83.5(5)°] and N(4)–Cu–N(3) [83.6(17)°] bond angles are lower than 90° because of the steric crowding presented by the 1,4-diazepane backbone.

Electronic and EPR Spectral Studies. The absorption spectra of 1–6 exhibited broad bands around 583–730 nm in the solid state, which correspond to the d–d transitions (Figure S1 and Table S1).³⁸ In an CH₃CN solution, they appeared around 582–757 nm with smaller ϵ values (171–280 M^{−1} cm^{−1}; Figure S2 and Table S1). The shoulders around 296–309 nm and transitions around 237–264 nm correspond to $\pi \rightarrow \pi^*$ transitions of the ligands.^{35,39–41} These filled ligand-based molecular orbitals at higher energy may be excited into the partially filled e_g orbital set and caused the ligand-to-metal charge-transfer (LMCT) transitions.^{42,43} The positions of the d–d bands suggest the existence of five-coordination geometry around the copper(II) center (Figures S2 and S3 and Table S1).^{35,41} They appeared to be a combination of two transitions, $d_{x^2-y^2} \rightarrow d_{xz}$, d_{yz} and $d_{x^2-y^2} \rightarrow d_z^2$. This may have originated from the interconversion of TBP and SP coordination geometries, which is known to occur in solution via changes in the ligand field (LF) at the z direction and by changing the equatorial-plane LF.^{42,43} Thus, it resulted in the ground state being a combination of $d_{x^2-y^2}$ and d_z^2 and consequently in a change of the d–d band positions from the value expected for a perfect TBP/SP geometry.^{42,43}

The geometry of the copper(II) center is directly associated with the energy of the d–d transitions. The d–d bands around 586–620 nm for 4–6 possibly correspond to more SP geometry.^{35,39,40} Interestingly, the addition of Et₃N caused the shift of d–d bands to low energy (734–745 nm) along with formation of the shoulder around 590–630 nm (Figures S4 and S5). Therefore, the addition of Et₃N appears to alter the coordination geometry and is believed to exhibit mixed SP and TBP geometries in solution.^{35,42} All four nitrogen donors of L4–L6 support SP geometry in CH₃CN; however, the addition of a base may result in the decoordination of one of the pyridyl arms. This likely facilitated the interconversion of TBP or less SP geometry,^{35,42,43} which is predominantly noticed for 6 than 4 and 5 and correlates to the catalytic activity differences (cf. below). This geometrical interconversion may be fast, and no clear isosbestic points were noticed for these complexes. Solomon et al. rationalized that the five-coordination geometry normally undergoes an interconversion of SP to TBP geometry and vice versa via either a C_{2v} distortion (Berry pseudorotation) or a C_s distortion. The second conversion is associated with ligand displacement reactions in the square plane, wherein an axial ligand switches to the plane for displacement of a ligand equatorial site.^{35,43} There was no significant shift of d–d transitions caused by 1–3 with Et₃N due to the absence of major structural rearrangements. These complexes adopted more TBP even without the addition of a base (Figure S4).

Electron paramagnetic resonance (EPR) spectra were measured at 70 K using a mixture (8:2) of solvents methanol and N,N-dimethylformamide (DMF). The hyperfine splitting was discerned in the parallel region (g_{\parallel}) for all complexes (Figure 2 and Table S1). Complexes 1–3 displayed g_{\parallel} values of 2.245–2.250. The f values were calculated as 151–154 cm^{−1}

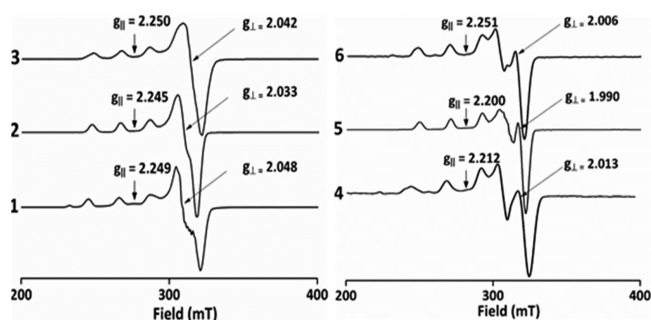


Figure 2. EPR spectra of 1–6 at 70 K in methanol/DMF (8:2) and g values provided on each spectra. Frequencies: 1, 9.00903 GHz; 2, 9.00743 GHz; 3, 9.00851 GHz; 4, 9.01365 GHz; 5, 9.01277 GHz; 6, 9.01523 GHz. Power = 0.99 mW; modulation frequency = 100 kHz; modulation amplitude = 10 G; $T = 70$ K.

and are higher than $105\text{--}135\text{ cm}^{-1}$, which is expected for geometries with a square base.^{43–45} It indicates that the geometry is strongly distorted and deviated from planarity to form a TBP geometry.^{43–45} Thus, the ground state appears to be the mixing of $d_{x^2-y^2}$ and d_{z^2} orbitals.⁴⁴ It is further supported by the lower hyperfine coupling constant values (A_{\parallel}), $(146\text{--}149) \times 10^{-4}\text{ cm}^{-1}$, which are closer to the A_{\parallel} values reported for the TBP geometry.⁴⁵ Conversely, complexes 4–6 showed g_{\parallel} (2.200–2.251) $>$ g_{\perp} (1.990–2.013) and f values of $133\text{--}142\text{ cm}^{-1}$ and are comparable to the values reported for geometries with a square-planar base (cf. above).^{43–45} The larger A_{\parallel} value of $(159\text{--}166) \times 10^{-4}\text{ cm}^{-1}$ further supports the SP geometry.^{44,45} The minor g components 2.556 for 1, 2.613, 2.504, and 2.425 for 4 and 2.532 and 2.415 for 6 are possibly ascribed to the minor species that may have been generated during solvation⁴⁶ or geometrical interconversions (cf. above).⁴⁶ However, these minor species values are significantly different from values obtained for $\text{Cu}(\text{ClO}_4)_2 \cdot 6\text{H}_2\text{O}$. The hyperfine coupling of a d electron with copper(II) nuclear spin has perhaps contributed via lower Fermi contact, spin dipolar and orbital dipolar.⁴⁵ The SO_3CF_3^- derivatives of the complexes displayed EPR spectral parameters almost identical with those of their respective perchlorate complexes.⁴⁵

Table 2. Catalytic Benzene Hydroxylation

cat. ^a	[C] ^b (%)	[Y] ^c (%)	[S] ^d (%)	TON ^e	TOF ^f (h ⁻¹)	KIE ^g	k_{obs} ($\times 10^{-2}\text{ s}^{-1}$) ⁱ
1	41	32 ± 0.5	76	640 ± 10	128	0.97	7.51 ± 0.004
1a	42	33 ± 0.3	78	660 ± 6	132		
2	36	34 ± 0.8	96	680 ± 16	136	0.99	9.29 ± 0.002
2a	37	35 ± 1.0	94	700 ± 20	140		
3	37	37 ± 0.5	98	740 ± 16	148	0.98	11.85 ± 0.002
3a	38	38 ± 1.3	98	760 ± 26	152	1.08 ^h	6.26 ± 0.004 ^j
4	46	25 ± 0.5	56	500 ± 10	100	1.04	
4a	47	27 ± 0.2	58	540 ± 4	108		
5	44	17 ± 0.8	39	340 ± 16	68	0.98	
5a	45	18 ± 1.0	40	360 ± 20	72		
6	49	29 ± 0.3	60	580 ± 6	116	1.12	2.54 ± 0.01
6a	50	32 ± 0.6	63	640 ± 12	128		

^aReaction conditions: substrate (5 mmol), catalyst (2.5 μmol , 0.05%), Et_3N (2.5 μmol), and 30% H_2O_2 (25 mmol) in CH_3CN for 5 h. ^bConversion. ^cYield (reported values represent the mean value of three reactions). ^dSelectivity. ^eTurnover number. ^fTurnover frequency. ^gCatalyst (2.5 μmol), a 1:1 mixture of C_6D_6 (0.25 mmol) and C_6H_6 (0.25 mmol), and 30% H_2O_2 (2.5 mmol) at 60 °C for 5 h. ^hKIE observed for the reaction of a 1:1 mixture of C_6D_6 and C_6H_6 with $[\text{CuL3}(\text{OOH})]^+$ ($1 \times 10^{-4}\text{ M}$ in CH_3CN). ⁱThe spectral changes observed for 1–6 ($1 \times 10^{-4}\text{ M}$) with 10 equiv of H_2O_2 and Et_3N (1 equiv) in CH_3CN at -40 °C. ^jThe spectral changes for the reaction of $[\text{CuL3}(\text{OOH})]^+$ ($1 \times 10^{-4}\text{ M}$) and benzene (50 equiv) in CH_3CN at -40 °C.

The covalencies of in-plane σ bonds (α^2), in-plane π bonds (β^2), and out-of-plane π bonds (γ^2) were estimated from the EPR data and d–d transitions.^{45,47} Complexes 1–6 exhibited α^2 (0.690–0.731), β^2 (0.992–1.110), and γ^2 (0.264–0.956) covalencies (Table S1), where ionic bonding has α^2 values near to 1, and this value has a reciprocal correlation with covalent character. The orbital reduction parameters $K_{\parallel} = \alpha^2\beta^2$ and $K_{\perp} = \alpha^2\gamma^2$ were calculated as 0.699–0.800 and 0.193–0.688, respectively. Complexes 1–6 exhibited $K_{\parallel} > K_{\perp}$, which reveals the existence of a remarkable quantity of π bonding at the outer plane. The pure σ -bonding $K_{\parallel} = K_{\perp}$ and the π -bonding $K_{\parallel} < K_{\perp}$ in the plane have been described in the literature.⁴⁴

Redox Properties. The redox potentials of the complexes were studied by cyclic voltammetry using a three-electrode setup and the supporting electrolyte NBu_4PF_6 in CH_3CN . The redox couple $\text{Cu}^{\text{II}}/\text{Cu}^{\text{I}}$ has been observed at a negative potential range for 1–6 (Figure S6 and Tables S1 and S2). The redox potential of -0.251 V for 1 is more positive compared to those of complexes 2 (-0.351 V) and 3 (-0.383 V). The more negative redox potential of 3 may be imposed by the electron-releasing $-\text{Me}$ and $-\text{OMe}$ groups. These redox potentials are higher than those of 4 (-0.513 V), 5 (-0.450 V), and 6 (-0.527 V) versus Ag/Ag^+ . The ΔE values of 1 (86 mV) and 3 (83 mV) are slightly away from reversibility; however, 2 showed a redox couple far away from reversibility (ΔE , 134 mV). The redox couple of 4 is close to reversibility (ΔE , 77 mV), but 5 (ΔE , 158 mV) and 6 (ΔE , 150 mV) showed redox couples far away from reversibility. Thus, the structural and electronic variations of the ligands appear to influence the redox potential. Further, the SO_3CF_3^- derivatives 1a–6a exhibited redox behavior almost identical with that of their respective perchlorate complexes (Figure S7 and Tables S1 and S2). The order of the redox potential is $1 > 2 > 3 > 5 > 4 > 6$.

Benzene Hydroxylation Reactions. Hydroxylation of benzene was performed using copper(II) complexes as catalysts and H_2O_2 (30%) as the oxygen source at 60 °C. The reaction condition was optimized using 3 (see details in Table S3). Under optimized conditions, 5 mmol of benzene (0.45 mL) and 0.05 mol % copper(II) complex (2.5 μmol) were mixed in CH_3CN (2.0 mL). Further, the base Et_3N (2.5

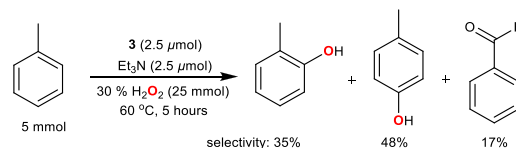
μmol) and aqueous 30% H_2O_2 (25 mmol) were added gradually, and the reactions were performed for 5 h. Finally, the solution was passed via a silica column for removal of the catalyst and subsequently subjected to gas chromatography (GC)–mass spectrometry (MS)/GC analyses (Figures S8 and S9 and Table 2). Complex 1 exhibited phenol formation of 32% and a TON of 640, wherein 76% of selectivity was achieved. Replacement of the ethylene chain in 1 by a propylene chain led to 2, which showed a slightly enhanced phenol yield of 34%, a TON of 680, and a much better selectivity of 96%. Further introducing electron-donor groups on pyridine arms to obtain complex 3 showed a better catalytic efficiency than 1 and 2. It afforded a phenol yield of 37% with a TON of 740 and an improved selectivity of 98%. The spacer connected to the $-\text{NMe}_2$ group and electron-donating groups on pyridines influences significantly for the variation of the catalytic efficiency. On the other hand, the catalyst 4 showed a significant decrease in phenol formation (25%) and selectivity (56%) (Table 2) over those of 1–3. This catalytic efficiency further declines by replacing pyridines in 4 by a quinoline arm to attain 5, which displayed the lowest phenol yield (17%), TON (340), and selectivity (39%) among the series. The increase of the chelate ring size as in 6 showed moderately increased phenol yield (29%), TON (580), and selectivity (60%) over those of 4 and 5. The decreasing order of the catalytic power of the complexes is observed as $3 > 2 > 1 > 6 > 4 > 5$. The replacement of the tripodal backbone by a sterically crowded cyclic diazepane unit results in a decrease of the catalytic efficiency.

Benzene hydroxylation reactions have been performed for SO_3CF_3^- -containing complexes (1a–6a) under identical reaction conditions to understand the role of the counterion. Complex 1a showed 33% of phenol formation and a TON of 660, wherein 78% of selectivity was achieved. Similarly, complexes 2a–6a showed the slightly different phenol yields at 60 °C: 2a, 35%; 3a, 38%; 4a, 27%; 5a, 18%; 6a, 32%. The results advocate that a change of the counterion is not significantly affected by the phenol yield and catalytic power (Table 2). The currently observed catalytic efficiency is significantly higher than those in the previous report by Kodera et al., where 22% conversion of benzene to a mixture of products (phenol and *p*-benzoquinone) has been attained at 50 °C over 40 h.³⁰ The copper(II) complexes of tripodal ligand scaffolds are found to be more efficient than the cyclic 1,4-diazepane support. This difference likely originated from the geometries of complexes and their catalytically active intermediates $[(\text{L})\text{CuOOH}]^+$ (cf. below). Complexes 1–3 adopted more TBP coordination geometry and are expected to stabilize almost identical geometry for $[(\text{L})\text{CuOOH}]^+$,⁴⁸ whereas diazepane-based ligands L4 and L5 support more SP geometry in 4 and 5. The additional methylene group connecting pyridine and diazepane units in 6 possibly enforces geometry between TBP and SP and is likely responsible for a better yield of phenol than complexes 4 and 5 (cf. above). The ligand L3 showed a more steric nature with the highest % V_{bur} of 75.2% than L1 and L2 (Figure S10). This steric crowding is also directly associated with the highest catalytic efficiency of L3 among tripodal ligand complexes.⁴⁹

The benzene hydroxylation reactions were also carried out at 25 °C (Table 2), where the catalyst 1 displayed 12% yield of phenol and a TON of 240. Similarly, other complexes were also afforded phenol formation: 2, 13%; 3, 16%; 4, 9%; 5, 5% and 6, 11% (Table S4). These yields are relatively smaller than

those observed at elevated temperature (60 °C) for all complexes, but the trends of the reactivity are found to be identical. These yields are higher than those of the other reported complexes at room temperature.³¹ The stoichiometric reaction of 3, benzene, and H_2O_2 afforded 21% yield of phenol with a selectivity of 52%, and a significant amount of *p*-benzoquinone (20%) was also observed (Figure S11). The catalytic reactions using more than 1 equiv of Et_3N showed neither inhibition nor acceleration of the product yield. However, less than 1 equiv of Et_3N showed a decreased yield of phenol formation (26%). Interestingly, the bulk-scale catalytic reaction using the most efficient catalyst 3 exhibited phenol formation of up to 0.441 g (4.7 mmol) at 60 °C over 48 h. Besides, the catalytic reaction using O_2 instead of H_2O_2 displayed a decreased phenol yield (9%) with a selectivity >99% at 60 °C for 24 h, while employing *tert*-butyl hydroperoxide as an oxygen source showed 16% yield of phenol under identical reaction conditions. Further, the reaction of phenol (5 mmol) as the substrate and 3 as the catalyst exhibited no hydroxylated product at 60 °C, and the substrate was recovered almost quantitatively. This is strongly revealing that the catalysts are proficient in executing monohydroxylation of the aromatic C–H bond selectively, without any overoxidation. Also, toluene and ethylbenzene were used as the substrates to study the C–H functionalization ability of alkyl versus aromatic bonds. Toluene showed the formation of *o*- and *p*-cresol (yield of 8%; selectivity of 83%) and benzaldehyde (yield of <1%; selectivity of 17%) without quinone formation at 60 °C (Scheme 2). It suggests that the

Scheme 2. Catalytic Hydroxylation of Toluene by 3



aromatic sp^2 carbon preferably functionalized, and similar observations were reported in the literature,⁵⁰ whereas the use of the substrate ethylbenzene displayed selective functionalization of sp^2 carbon and afforded 2.1% of ethylphenol formation but with the huge declined selectivity (48%) and without quinone formation. Cumene showed the formation of a mixture of substituted isopropyl phenol (yield, 6%) and <1% 2-phenyl-2-propanol (Scheme S1). Anisole afforded *o*-, *m*-, and *p*-methoxyphenols as products with a collective yield of 4% (Scheme S2). 1-Chlorobenzene showed the formation of a mixture of chlorophenols (4%; Scheme S3). The substrate nitrobenzene exhibited 5% formation of a mixture of nitrophenols (Scheme S4).

Mechanism of Benzene Hydroxylation. Kinetic isotope effect (KIE) has been investigated using complexes (2.5 μmol), a mixture of C_6D_6 (0.25 mmol) and C_6H_6 (0.25 mmol), as substrates under the conditions specified in Table 2. The KIE values were determined from the phenol to phenol- d_5 ratio by the GC–MS/GC method (Figure S12 and Table 2). The calculated KIE values of 0.97–1.12 for 1–6 are within the confines of values described for intramolecular aromatic hydroxylation (0.99–1.10).⁵¹ The metal-bound oxygen key intermediates are known to display a KIE value of ~ 1.0 for aromatic hydroxylation via an electrophilic aromatic substitution reaction.⁵¹ Further, these observations suggest that

breakage of the C–H bond is unlikely to be the rate-determining factor. The observed KIE values support that Fenton (1.7)⁵² or copper-insertion-type (2.9–4.8) reactions may not be followed.⁵³ In addition, KIE values were determined over various time intervals for **3** and showed KIE values of ~ 1.0 throughout the reaction time (Figure S13), which are almost similar to values obtained after 5 h. The use of excess substrate (1 mmol, 4 equiv to oxidant) with a limited amount of H₂O₂ (0.25 mmol) displayed KIE of 1.12, which is comparable to the above observations (Figure S14). The isotope-labeling experiments were executed for the most active catalyst **3** by utilizing 90% atom purity H₂¹⁸O₂ in water and keeping the other reaction conditions the same. It showed that 92% of ¹⁸O insertion into phenol (Figure S15). However, the use of H₂¹⁸O and H₂O₂ showed almost no ¹⁸O-atom-incorporated phenol product. These results suggest that the utilization of H₂O₂ is crucial for the transformation of benzene to phenol.⁵⁴

Intriguingly, the reaction of **3** with 30% H₂O₂ (10 equiv) and 1 equiv of Et₃N exhibited O (π^*_o) \rightarrow Cu LMCT transition⁵⁵ at 390 nm in CH₃CN at -40 °C, which may correspond to the Cu^{II}-OOH intermediate (Figure 3). The base Et₃N has seemingly facilitated the binding of H₂O₂ with the copper(II) center. The rate of formation of the species was

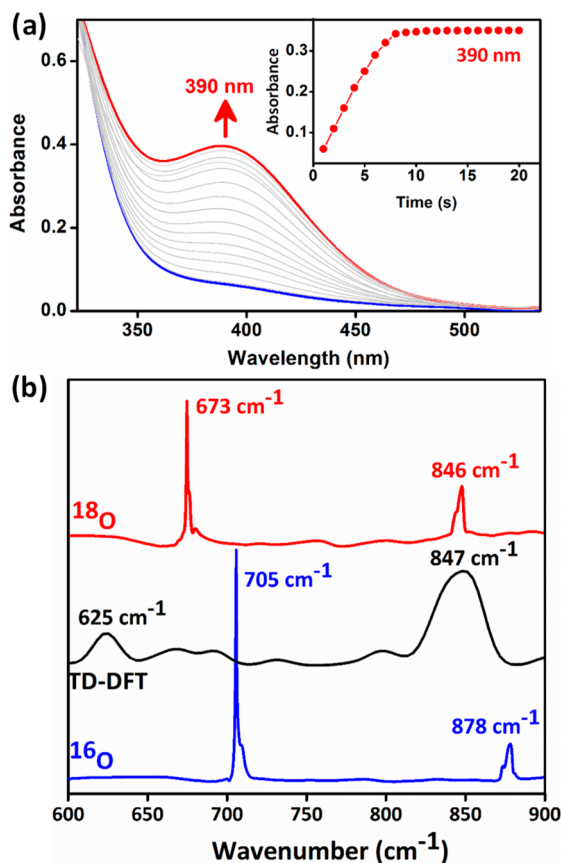


Figure 3. (a) Electronic spectral changes for the reaction of **3** (1×10^{-4} M) with 10 equiv of H₂O₂ and Et₃N (1 equiv) in CH₃CN at -40 °C. Inset: Plot of time versus absorbance at 390 nm. (b) Solution FT-IR spectra of [Cu^{II}.¹⁶O¹⁶OH] species (blue) and [Cu^{II}.¹⁸O¹⁸OH] species (red) obtained by the reaction of **3** (1×10^{-4} M) and 10 equiv of H₂¹⁶O₂ and H₂¹⁸O₂, respectively, in the presence of Et₃N (1 equiv) in CH₃CN. The calculated vibrational spectra of [CuL3-(OOH)]⁺ by TD-DFT (black).

calculated as $(11.85 \pm 0.002) \times 10^{-2} \text{ s}^{-1}$ ($t_{1/2}$, 58 s) from the growth of this LMCT band (Figure S16 and Table 2). The time-dependent DFT (TD-DFT) calculation showed the energy of the oxo-to-copper(II) LMCT transition at 366 nm and supports the experimental observation. The solution Fourier transform infrared (FT-IR) spectral studies further supported our predictions, and the stretching frequencies of the Cu–O and O–O bonds appeared at 705 and 878 cm⁻¹, respectively. They were shifted to 673 and 846 cm⁻¹ when using H₂¹⁸O₂ (90% atom purity) instead of H₂¹⁶O₂ (Figure 3). The observed isotopic shift $^{16}\Delta - ^{18}\Delta = 32 \text{ cm}^{-1}$ is comparable to those of other structurally and spectroscopically well-characterized Cu^{II}-OOH species.⁵⁶ The calculated vibration spectra of Cu^{II}-OOH species showed stretching frequencies at 625 cm⁻¹ corresponding to the Cu–O bond and 847 cm⁻¹ for the O–O bond, which look very near to the experimentally observed values (Figure 3). Notably, these vibrational frequency values are lower than those of copper superoxo (Cu-OO*) intermediates, wherein the values for side-on Cu-OO* and end-on Cu-OO* species are reported at 1043 and 1122 cm⁻¹, respectively, with $\nu(\text{Cu}-\text{O})$ around 422–474 cm⁻¹.⁵⁷ Further, the addition of 50 equiv of benzene to [(L3)Cu^{II}-OOH]⁺ species showed that the disappearance of vibrational frequencies at 705 and 878 cm⁻¹ corresponds to the Cu–O and O–O bonds, respectively, and supports involvement of the Cu^{II}-OOH putative intermediate.⁵⁷ On the other hand, warming up the solution to room temperature showed the disappearance of these vibrational frequencies. The mass spectral (ESI-MS) analysis of the species displayed m/z 496.00 (calcd m/z 496.21) in CH₃CN, which corresponds to [(L3)Cu^{II}-OOH]⁺ (Figure S17). Remarkably, the addition of benzene (50 equiv) to [(L3)Cu^{II}-OOH]⁺ at -40 °C in CH₃CN leads to the instant collapse of species with the pseudo-first-order reaction profile. This decay has coexisted with the vanishing of the LMCT band (Figure 4). The decay

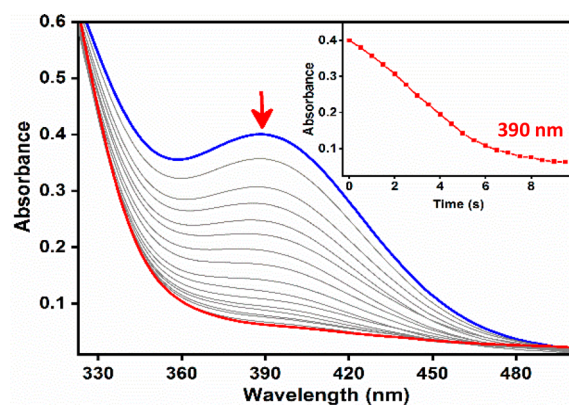


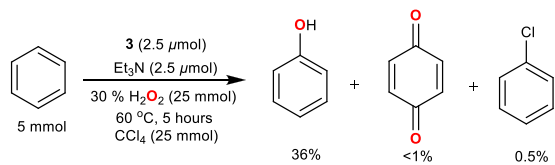
Figure 4. Reaction of [CuL3(OOH)]⁺ (1×10^{-4} M) with benzene (50 equiv) in CH₃CN at -40 °C and its electronic spectral changes. Time interval: 1 s. Inset: Plot of time versus absorbance at 390 nm.

constant has been determined as $k_1 = (6.26 \pm 0.004) \times 10^{-2} \text{ s}^{-1}$ (Figure S18). The plot of the first-order rate constants versus various amounts of benzene showed a linear correlation to obtain the second-order rate constant $k_2 = 2.7 \pm 0.009 \times 10^{-2} \text{ s}^{-1}$ (Figure S19). Product analysis for this reaction showed the formation of phenol selectively. Also, KIE values were determined from the kinetics by adding a mixture (1:1) of benzene-*d*₆ and benzene to [(L3)Cu^{II}-OOH]⁺ species at -40 °C in CH₃CN. The KIE was calculated as 1.08 by GC-

MS/GC investigations after complete decay of the LMCT band (Figure S20 and Table 2), which is consistent with the earlier observations.

Benzene hydroxylation performed using the catalyst **3** and the radical trapping agent 2,2,6,6-tetramethylpiperidin-1-yl-oxyl exhibited no distinguishable change in the phenol yield at 60 °C. This result eradicates the possibility of the radical-type reaction mechanism.⁵⁸ The use of another radical trapping agent, dimethylpyrroline *N*-oxide (DMPO), was not suggested helpful information, where more or less equal quantities of DMPO–OH radicals have been determined by EPR with or without the use of a catalyst. The oxidation of the substrate *cis*-1,2-dimethylcyclohexane has been carried out under an optimized reaction condition using **3** as the catalyst, which showed 12.6% of the *cis*-hydroxylated product with a trace of *trans* product (<1%; Figure S21). This stereoretention of C–H oxidation reactions indicates that Fenton-type species are unlikely involved,⁵⁹ which supports our earlier prediction by KIE (cf. above). Besides, the use of CCl₄ as a trapping agent afforded 96% and 4% selectivity of phenol (including the benzoquinone byproduct) and chlorobenzene, respectively (Scheme 3 and Figure S22). This suggests that the use of CCl₄

Scheme 3. Benzene Hydroxylation by **3** in the Presence of CCl₄



does not significantly affect the selectivity of phenol and eliminates the possibility of the Fenton-type reaction pathway.⁶⁰ The reaction without catalysts has not afforded any amount of chlorobenzene formation. In another experiment, cyclohexane was used as the substrate, **3** as the catalyst, and CCl₄ as the radical trapping agent, where 95% selectivity of cyclohexanol and cyclohexanone formation with 5% of cyclohexyl chloride was observed (Figure S23), which again supports exclusion of the possibility of the radical-type reaction pathway.²⁹

Similarly, the species [(L)Cu^{II}-OOH]⁺ of **1**, **2**, and **4** and **5** have been obtained by the reaction of respective complexes with 30% H₂O₂ (10 equiv) and 1 equiv of Et₃N at –40 °C in CH₃CN. They showed almost similar electronic spectral signatures and kinetic behaviors: **1**, λ_{max} 380 nm; k_{obs} (7.51 ± 0.004) × 10^{–2} s^{–1}, and t_{1/2} 91 s; **2**, λ_{max} 370 nm; k_{obs} (9.29 ± 0.002) × 10^{–2} s^{–1}, and t_{1/2} 74 s; **6**, λ_{max} 375 nm; k_{obs} (2.54 ± 0.01) × 10^{–2} s^{–1}, and t_{1/2} 27 s (Figures S24–S26). Further, the formation of these [(L)Cu^{II}-OOH]⁺ species was confirmed by ESI-MS spectra: *m/z* 366.20 (calcd *m/z* 366.11) correspond to [(L1)Cu^{II}-OOH]⁺; *m/z* 379.80 (calcd *m/z* 380.12) for [(L2)Cu^{II}-OOH]⁺; *m/z* 378.40 (calcd *m/z* 378.11) for [(L4)Cu^{II}-OOH]⁺; *m/z* 405.8 (calcd *m/z* 406.14) for [(L6)Cu^{II}-OOH]⁺ (Figures S27–S30). However, characterization of the intermediate of **5** has been unproductive in spite of constant efforts because it likely to have a very short lifetime.

Repeated attempts to isolate single crystals of species [(L)Cu^{II}-OOH]⁺ were unsuccessful for all complexes under various conditions. However, the geometry of intermediate

[(L3)Cu^{II}-OOH]⁺ has been optimized by DFT calculations.⁶¹ The calculations were performed using split valence basic sets (def2-SVP and def2-TZVP for all atoms).⁶¹ The calculated Cu–O (1.8981 Å) and O–O (1.4310 Å) bond distances are closer to the previously reported values determined from crystal structures of copper(II) hydroperoxo complexes (Cu–O, 1.888 Å; O–O, 1.460 Å).⁶² The optimized structure of [(L3)Cu^{II}-OOH]⁺ revealed a distorted TBP geometry (τ, 0.64), where the –OOH group occupied an axial site, which is comparable to the previous reports (Figure 5 and Table S5).^{62–64}

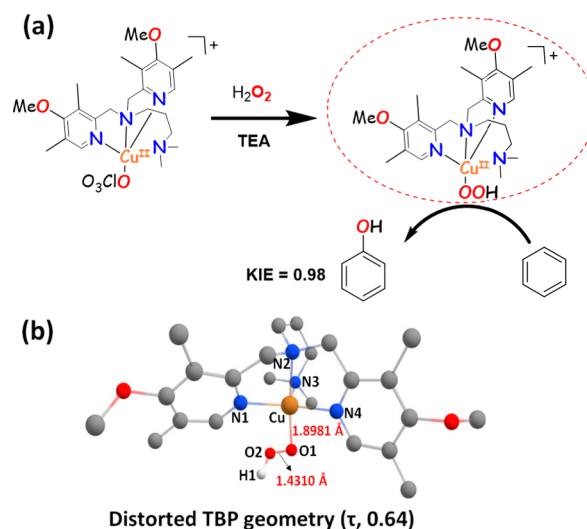


Figure 5. (a) Catalytic benzene hydroxylation by **3** and H₂O₂. (b) Optimized structure of [(L3)Cu^{II}-OOH]⁺ by DFT using B3LYP/def2-SVP and def2-TZVP basis sets.

CONCLUSIONS

Bioinspired copper(II) complexes of N₄ ligands have been reported as catalysts for direct benzene hydroxylation. The molecular structures of tripodal ligand-based complexes exhibited more TBP geometry; however, diazepane-based complexes adopted more SP geometry. All catalysts showed benzene hydroxylation to form phenol selectively by utilizing H₂O₂ as an oxidant at 25/60 °C, and no overoxidized products were observed. The complexes with more TBP geometry showed the highest catalytic efficiency (37% yield of phenol) and selectivity (98%). However, the diazepane-based complexes with more SP displayed comparatively reduced yields and poor selectivity. The hydroxylation reaction mechanism likely proceeds via Cu^{II}-OOH species, and they were characterized by various spectroscopies and supported by DFT and TD-DFT calculations. The KIE investigations support the involvement of Cu–O₂ species. The oxygen isotope-labeling studies indicate that H₂O₂ is the crucial oxygen atom supplier to form phenol. The coordination geometry of the copper(II) center directly impacts the catalysis, as evidenced by the fact that more TBP-based geometry of complexes better supports the generation of Cu^{II}-OOH species and higher yield of phenol and selectivity. The coordination geometry of Cu^{II}-OOH species was optimized as distorted TBP.

EXPERIMENTAL SECTION

Synthesis of Ligands. The present ligands L1–L6 have been synthesized as reported previously.^{32–34} **Caution!** Copper(II) perchlorate salt with ligands should be handled carefully due to possible explosion.

Synthesis of Copper(II) Complexes (1–6). The copper(II) complexes were synthesized by a known procedure.³⁵ The solution of $\text{Cu}(\text{ClO}_4)_2 \cdot 6\text{H}_2\text{O}$ (0.185 g, 0.5 mmol) in methanol (5 mL) was added dropwise to the ligands (0.5 mmol) in methanol (20 mL). The reaction mixtures were stirred for 3 h at 25 °C. The color of the solutions turned blue, and removal of the solvent afforded blue residues, which were washed twice with hexane (2×10 mL) to remove the excess ligand. The complexes were dried under high vacuum over fused CaCl_2 .

The complexes $[\text{Cu}(\text{L})(\text{SO}_3\text{CF}_3)]\text{SO}_3\text{CF}_3$ (**1a–6a**) were isolated as blue solids using $\text{Cu}(\text{CF}_3\text{SO}_3)_2$ as the starting material, as reported previously.³⁵ Suitable blue crystals of **2a** and **4a** for single-crystals X-ray crystallographic studies were isolated by diethyl ether diffusion into a CH_3CN solution of the respective complexes.

$[\text{Cu}(\text{L1})(\text{ClO}_4)]\text{ClO}_4$ (**1**). Yield: 0.27 g (86%). Analytically calculated elements for $\text{C}_{16}\text{H}_{22}\text{CuN}_4\text{O}_8\text{Cl}_2$: C, 36.07; H, 4.16; N, 10.52. Found: C, 36.04; H, 4.12; N, 10.48. ESI-MS (m/z): 432.06 ($[\text{M} - \text{ClO}_4]^+$).

$[\text{Cu}(\text{L2})(\text{ClO}_4)]\text{ClO}_4$ (**2**). Yield: 0.23 g (81%). Analytically calculated elements for $\text{C}_{17}\text{H}_{24}\text{CuN}_4\text{O}_8\text{Cl}_2$: C, 37.34; H, 4.42; N, 10.25. Found: C, 37.28; H, 4.37; N, 10.21. ESI-MS (m/z): 446.07 ($[\text{M} - \text{ClO}_4]^+$).

$[\text{Cu}(\text{L3})(\text{ClO}_4)]\text{ClO}_4$ (**3**). Yield: 0.19 g (74%). Analytically calculated elements for $\text{C}_{23}\text{H}_{36}\text{CuN}_4\text{O}_{10}\text{Cl}_2$: C, 41.67; H, 5.47; N, 8.45. Found: C, 41.63; H, 5.45; N, 8.42. ESI-MS (m/z): 562.16 ($[\text{M} - \text{ClO}_4]^+$).

$[\text{Cu}(\text{L4})(\text{ClO}_4)]\text{ClO}_4$ (**4**). Yield: 0.28 g (91%). Analytically calculated elements for $\text{C}_{17}\text{H}_{22}\text{CuN}_4\text{O}_8\text{Cl}_2$: C, 37.48; H, 4.07; N, 10.28. Found: C, 37.53; H, 3.85; N, 10.25. ESI-MS (m/z): 444.03 ($[\text{M} - \text{ClO}_4]^+$).

$[\text{Cu}(\text{L5})(\text{ClO}_4)]\text{ClO}_4$ (**5**). Yield: 0.17 g (65%). Analytically calculated elements for $\text{C}_{25}\text{H}_{26}\text{CuN}_4\text{O}_8\text{Cl}_2$: C, 46.56; H, 4.06; N, 8.69. Found: C, 46.51; H, 4.02; N, 8.65. ESI-MS (m/z): 544.09 ($[\text{M} - \text{ClO}_4]^+$).

$[\text{Cu}(\text{L6})(\text{ClO}_4)]\text{ClO}_4$ (**6**). Yield: 0.26 g (89%). Analytically calculated elements for $\text{C}_{19}\text{H}_{26}\text{CuN}_4\text{O}_8\text{Cl}_2$: C, 39.84; H, 4.57; N, 9.78. Found: C, 40.03; H, 4.88; N, 9.63. ESI-MS (m/z): 472.67 ($[\text{M} - \text{ClO}_4]^+$).

Procedure for Benzene Hydroxylation. The complex $[\text{Cu}(\text{L})-(\text{ClO}_4)]\text{ClO}_4$ (2.5 μmol) and benzene (5.0 mmol) were mixed in CH_3CN (2.0 mL). Then, 30% H_2O_2 (2.5 mL, 25 mmol) and Et_3N (2.5 μmol) were added very slowly to the reaction mixture. The stirring was continued at 60/25 °C for 5 h. After cooling to room temperature, the catalyst was removed by passing through a solution on silica gel. A known amount of nitrobenzene was added as an internal standard. The conversion and yield of the reaction were determined with GC–MS/GC.

Determination of the Kinetic Deuterium Isotope Effect (KIE). A mixture of the substrate benzene (0.25 mmol) and benzene- d_6 (0.25 mmol) was added to a solution of the copper(II) complex (2.5 μmol) in CH_3CN (2 mL). Then, 30% H_2O_2 (0.50 mL) and Et_3N (2.5 μmol) were added slowly to the reaction mixture under constant stirring, which was continued for an additional 5 h at 60 °C. Finally, the reaction mixture passed through a solution on silica gel to remove the complex. The product distribution was calculated by GC–MS/GC analysis. The KIE value was calculated from the ratio of phenol and phenol- d_5 .

Isotopic Labeling Studies Using $\text{H}_2^{18}\text{O}_2$ and H_2^{18}O and Kinetic Measurements. All of these experiments were performed as reported previously by us with suitable modifications.^{11c} Details of the experiments are provided in the Supporting Information.

Solution FT-IR Measurements. Solution-state FT-IR experiments were performed on a Thermo Nicolet 6700 spectrometer. The species of 3 $[\text{Cu}^{\text{II}}\text{O}^{16}\text{OH}]$ and $[\text{Cu}^{\text{II}}\text{O}^{18}\text{OH}]$ were freshly generated from 30% H_2O_2 and $\text{H}_2^{18}\text{O}_2$ (90% atom purity), respectively, in CH_3CN . Finally, solutions were carefully transferred to the CaF_2 cell via a microsyringe to measure the spectra.

Catalytic Hydroxylation of Other Substrates. The most active catalyst **3** (2.5 μmol) and appropriate substrates (5.0 mmol) were used and the reactions performed by keeping other procedures similar to that followed for benzene hydroxylation.

Radical Trapping Experiments Using CCl_4 . Catalytic amounts of **3** (2.5 μmol) and benzene (5.0 mmol) were dissolved in CH_3CN (2.0 mL). Then, 30% H_2O_2 (2.5 mL, 25 mmol), Et_3N (2.5 μmol), and CCl_4 (2.4 mL, 25 mmol) were slowly added to the reaction mixture. The solution was stirred at 60 °C for 5 h. After completion of the reaction, the usual workup and product analysis were followed, which was similar to that of benzene hydroxylation without CCl_4 .

DFT and TD-DFT Calculations. Optimization of the geometries was carried out by a DFT method. The electronic and vibrational spectra of key intermediates were calculated by TD-DFT. All of these calculations were performed by using double- ζ -quality split-valence basis sets with polarization functions (def2-SVP) and larger triple- ζ basis sets (def2-TZVP) for all atoms; TD-DFT calculations were also performed using B3LYP and def2-TZVP basis sets for all atoms, and calculations were carried out by ORCA 4.0.⁶⁵ The steric map calculations were performed by the SambVca 2.1A web application, which can be found at <https://www.molnac.unisa.it/OMtools/sambvca2.1/index.html>.⁴⁹

ASSOCIATED CONTENT

Supporting Information

The Supporting Information is available free of charge at <https://pubs.acs.org/doi/10.1021/acs.inorgchem.9b03676>.

Chemical details, physical methods (instrumentation), single-crystal X-ray diffraction measurement details, structural solution and refinements, other additional experimental methods, and additional spectral, redox, and kinetic data (PDF)

Accession Codes

CCDC 1959083 and 1959084 contain the supplementary crystallographic data for this paper. These data can be obtained free of charge via www.ccdc.cam.ac.uk/data_request/cif, or by emailing data_request@ccdc.cam.ac.uk, or by contacting The Cambridge Crystallographic Data Centre, 12 Union Road, Cambridge CB2 1EZ, UK; fax: +44 1223 336033.

AUTHOR INFORMATION

Corresponding Author

Ramasamy Mayilmurugan – *Bioinorganic Chemistry Laboratory/Physical Chemistry, School of Chemistry, Madurai Kamaraj University, Madurai 625021, India*; orcid.org/0000-0002-5370-594X; Email: mayilmurugan.chem@mkuniversity.org

Authors

Sethuraman Muthuramalingam – *Bioinorganic Chemistry Laboratory/Physical Chemistry, School of Chemistry, Madurai Kamaraj University, Madurai 625021, India*
Karunanithi Anandababu – *Bioinorganic Chemistry Laboratory/Physical Chemistry, School of Chemistry, Madurai Kamaraj University, Madurai 625021, India*
Marappan Velusamy – *Department of Chemistry, North Eastern Hill University, Shillong 793022, India*

Complete contact information is available at: <https://pubs.acs.org/doi/10.1021/acs.inorgchem.9b03676>

Notes

The authors declare no competing financial interest.

ACKNOWLEDGMENTS

We acknowledge the Science and Engineering Research Board, New Delhi, India, and Board of Research in Nuclear Science, Mumbai, India, for funding. S.M. sincerely acknowledges the Council of Scientific and Industrial Research, New Delhi,

India, for a Senior Research Fellowship [ref no. 09/114(0224)/19-EMR-I].

REFERENCES

- (1) Weissermel, K.; Arpe, H. J. *Industrial Organic Chemistry*, 3rd ed.; John Wiley & Sons, 2008.
- (2) Weber, M.; Kleine-Boymann, M. In *Ullmann's Encyclopedia of Industrial Chemistry*; Wiley-VCH: Weinheim, Germany, 2000.
- (3) Sheldon, R. A.; Kochi, J. K. In *Metal-Catalyzed Oxidations of Organic Compounds*; Sheldon, R. A., Kochi, J. K., Eds.; Academic Press: New York, 1981; pp 315–339.
- (4) Molinari, R.; Poerio, T. Remarks on Studies for Direct Production of Phenol in Conventional and Membrane Reactors. *Asia-Pac. J. Chem. Eng.* **2010**, *5*, 191–206.
- (5) (a) Schmidt, J. R. Industrial Catalytic Processes-Phenol Production. *Appl. Catal., A* **2005**, *280*, 89–103. (b) Borah, P.; Ma, X.; Nguyen, K. T.; Zhao, Y. A Vanadyl Complex Grafted to Periodic Mesoporous Organosilica: A Green Catalyst for Selective Hydroxylation of Benzene to Phenol. *Angew. Chem., Int. Ed.* **2012**, *51*, 7756–7761.
- (6) (a) Morrison, R.; Boyd, R. T. *Organic Chemistry*, 6th ed.; Prentice Hall: Englewood Cliffs, NJ, 1992. (b) Lee, B.; Naito, H.; Nagao, M.; Hibino, T. Alternating-Current Electrolysis for the Production of Phenol from Benzene. *Angew. Chem., Int. Ed.* **2012**, *51*, 6961–6965.
- (7) Xiao, F.; Sun, J.; Meng, X.; Yu, R.; Yuan, H.; Jiang, D.; Qiu, S.; Xu, R. A Novel Catalyst of Copper Hydroxyphosphate with High Activity in Wet Oxidation of Aromatics. *Appl. Catal., A* **2001**, *207*, 267–271.
- (8) Khatri, P. K.; Singh, B.; Jain, S. L.; Sain, B.; Sinha, A. K. Cyclotriphosphazene Grafted silica: A Novel Support for Immobilizing the Oxo-Vanadium Schiff Base Moieties for Hydroxylation of Benzene. *Chem. Commun.* **2011**, *47*, 1610–1612.
- (9) Shul'pin, G. B.; Kozlov, Y. N.; Shul'pina, L. S.; Carvalho, W. A.; Mandelli, D. Oxidation Reactions Catalyzed by Osmium Compounds. Part 4. Highly Efficient Oxidation of Hydrocarbons and Alcohols Including Glycerol by the H₂O₂/Os₃(CO)₁₂/pyridine reagent. *RSC Adv.* **2013**, *3*, 15065–15074.
- (10) Herron, N.; Tolman, C. A. A Highly Selective Zeolite Catalyst for Hydrocarbon Oxidation. A Completely Inorganic Mimic of the Alkane. Omega-Hydroxylases. *J. Am. Chem. Soc.* **1987**, *109*, 2837–2839.
- (11) (a) Bianchi, D.; D'Aloisio, R.; Bortolo, R.; Ricci, M. Oxidation of Mono- and Bicyclic Aromatic Compounds with Hydrogen Peroxide Catalyzed by Titanium Silicalites TS-1 and TS-1B. *Appl. Catal., A* **2007**, *327*, 295–299. (b) Pirutko, L. V.; Chernyavsky, V. S.; Uriarte, A. K.; Panov, G. I. Oxidation of Benzene to Phenol by Nitrous Oxide: Activity of Iron in Zeolite Matrices of Various Composition. *Appl. Catal., A* **2002**, *227*, 143–157. (c) Muthuramalingam, S.; Anandababu, K.; Velusamy, M.; Mayilmurugan, R. One Step Phenol Synthesis from Benzene Catalyzed by Nickel(II) Complexes. *Catal. Sci. Technol.* **2019**, *9*, 5991–6001.
- (12) (a) Lee, B.; Naito, H.; Hibino, T. Alternating-Current Electrolysis for the Production of Phenol from Benzene. *Angew. Chem., Int. Ed.* **2012**, *51*, 440–444. (b) Han, J. W.; Jung, J.; Lee, Y. M.; Nam, W.; Fukuzumi, S. Photocatalytic Oxidation of Benzene to Phenol Using Dioxygen as an Oxygen Source and Water as an Electron Source in the Presence of a Cobalt Catalyst. *Chem. Sci.* **2017**, *8*, 7119–7125. (c) Walling, C.; Johnson, R. A. Fenton's reagent. V. Hydroxylation and Side-chain Cleavage of Aromatics. *J. Am. Chem. Soc.* **1975**, *97*, 363–367.
- (13) (a) Balducci, L.; Bianchi, D.; Bortolo, R.; D'Aloisio, R. D.; Ricci, M.; Tassinari, R.; Ungarelli, R. Direct Oxidation of Benzene to Phenol with Hydrogen Peroxide over a Modified Titanium Silicalite. *Angew. Chem., Int. Ed.* **2003**, *42*, 4937–4940. (b) Nemati Kharat, A.; Moosavikia, S.; Tamaddoni Jahromi, B.; Badiei, A. Liquid Phase Hydroxylation of Benzene to Phenol over Vanadium Substituted Keggin Anion Supported on Amine Functionalized SBA-15. *J. Mol. Catal. A: Chem.* **2011**, *348*, 14–19.
- (14) Parida, K. M.; Rath, D. Structural Properties and Catalytic Oxidation of Benzene to Phenol over CuO-impregnated Mesoporous Silica. *Appl. Catal., A* **2007**, *321*, 101–108.
- (15) Song, S. Q.; Jiang, S. J.; Rao, R. C.; Yang, H. X.; Zhang, A. M. Bicomponent VO₂-defects/MWCNT Catalyst for Hydroxylation of Benzene to Phenol: Promoter Effect of Defects on Catalytic Performance. *Appl. Catal., A* **2011**, *401*, 215–219.
- (16) (a) Itoh, S.; Tachi, Y. Structure and O₂-reactivity of Copper(I) Complexes Supported by Pyridylalkylamine Ligands. *Dalton Trans.* **2006**, *38*, 4531–4538. (b) Nagataki, T.; Ishii, K.; Tachi, Y.; Itoh, S. Ligand effects on Ni^{II}-Catalysed Alkane-Hydroxylation with m-CPBA. *Dalton Trans.* **2007**, *11*, 1120–1128.
- (17) (a) Klinman, J. P. Mechanisms Whereby Mononuclear Copper Proteins Functionalize Organic Substrates. *Chem. Rev.* **1996**, *96*, 2541–2562. (b) Klinman, J. P. The Copper-Enzyme Family of Dopamine β -Monooxygenase and Peptidylglycine α -Hydroxylating Monooxygenase: Resolving the Chemical Pathway for Substrate Hydroxylation. *J. Biol. Chem.* **2006**, *281*, 3013–3016.
- (18) Prigge, S. T.; Mains, R. E.; Eipper, B. A.; Amzel, L. M. New Insights into Copper Monooxygenases and Peptide Amidation: Structure, Mechanism, and Function. *Cell. Mol. Life Sci.* **2000**, *57*, 1236–1259.
- (19) Halcrow, M. A. In *Comprehensive Coordination Chemistry II*; Que, J. L., Tolman, W. B., Eds.; Elsevier: Amsterdam, The Netherlands, 2004; Vol. 1, p 395.
- (20) Bollinger, J. M., Jr.; Krebs, C. Enzymatic C-H activation by Metal-Superoxo Intermediates. *Curr. Opin. Chem. Biol.* **2007**, *11*, 151–158.
- (21) (a) Hess, C. R.; Wu, Z.; Ng, A.; Gray, E. E.; McGuirl, M. A.; Klinman, J. P. Hydroxylase Activity of Met471Cys Tyramine β -Monooxygenase. *J. Am. Chem. Soc.* **2008**, *130*, 11939. (b) Melia, C.; Ferrer, S.; Rezáč, J.; Parisel, O.; Reinaud, O.; Moliner, V.; de la Londe, A. Investigation of the Hydroxylation Mechanism of Noncoupled Copper Oxygenases by Ab Initio Molecular Dynamics Simulations. *Chem. - Eur. J.* **2013**, *19*, 17328–17337.
- (22) Ortiz de Montellano, P. R. *Cytochrome P450: Structure, Mechanism, and Biochemistry*, 3rd ed.; Kluwer Academic/Plenum Publishers: New York, 2005.
- (23) Lieberman, R. L.; Rosenzweig, A. C. Biological Methane Oxidation: Regulation, Biochemistry, and Active Site Structure of Particulate Methane Monooxygenase. *Crit. Rev. Biochem. Mol. Biol.* **2004**, *39*, 147–164.
- (24) (a) Rolff, M.; Schottenheim, J.; Decker, H.; Tuzcek, F. Copper-O₂ Reactivity of Tyrosinase Models towards External Monophenolic Substrates: Molecular Mechanism and Comparison with the Enzyme. *Chem. Soc. Rev.* **2011**, *40*, 4077–4098. (b) Hamann, J. N.; Tuzcek, F. New Catalytic Model Systems of Tyrosinase: Fine-Tuning of the Reactivity with Pyrazole-based N-donor Ligands. *Chem. Commun.* **2014**, *50*, 2298.
- (25) (a) Itoh, S. Developing Mononuclear Copper-Active-Oxygen Complexes Relevant to Reactive Intermediates of Biological Oxidation Reactions. *Acc. Chem. Res.* **2015**, *48*, 2066–2074. (b) Kunishita, A.; Kubo, M.; Sugimoto, H.; Ogura, T.; Sato, K.; Takui, T.; Itoh, S. Mononuclear Copper(II)-Superoxo Complexes that Mimic the Structure and Reactivity of the Active Centers of PHM and D β M. *J. Am. Chem. Soc.* **2009**, *131*, 2788–2789. (c) Itoh, S.; Kondo, T.; Komatsu, M.; Ohshiro, Y.; Li, C.; Kanehisa, N.; Kai, Y.; Fukuzumi, S. Functional Model of Dopamine. β -Hydroxylase. Quantitative Ligand Hydroxylation at the Benzylic Position of a Copper Complex by Dioxygen. *J. Am. Chem. Soc.* **1995**, *117*, 4714–4715.
- (26) (a) Maiti, D.; Lee, D.-H.; Gaoutchenova, K.; Würtele, C.; Holthausen, M. C.; Narducci Sarjeant, A. A.; Sundermeyer, J.; Schindler, S.; Karlin, K. D. Reactions of a Copper(II) Superoxo Complex lead to C-H and O-H Substrate Oxygenation: Modeling Copper-Monooxygenase C-H Hydroxylation. *Angew. Chem., Int. Ed.* **2008**, *47*, 82–85. (b) Maiti, D.; Fry, H. C.; Woertink, J. S.; Vance, M. A.; Solomon, E. I.; Karlin, K. D. A 1:1 Copper-Dioxygen Adduct is an End-on Bound Superoxo Copper(II) Complex which Undergoes

Oxygenation Reactions with Phenols. *J. Am. Chem. Soc.* **2007**, *129*, 264–265. (c) Becker, M.; Schindler, S.; Karlin, K. D.; Kaden, T. A.; Kaderli, S.; Palanché, T.; Zuberbühler, A. D. Intramolecular Ligand Hydroxylation: Mechanistic High-Pressure Studies on the Reaction of a Dinuclear Copper(I) Complex with Dioxygen. *Inorg. Chem.* **1999**, *38*, 1989–1995. (d) Karlin, K. D.; Zhang, C. X.; Rheingold, A. L.; Galliker, B.; Kaderli, S.; Zuberbühler, A. D. Reversible Dioxygen Binding and Arene Hydroxylation Reactions: Kinetic and Thermodynamic Studies Involving Ligand Electronic and Structural Variations. *Inorg. Chim. Acta* **2012**, *389*, 138–150. (e) Ryan, S.; Adams, H.; Fenton, D. E.; Becker, M.; Schindler, S. Intramolecular Ligand Hydroxylation: Mechanistic Studies on the Reaction of a Copper(I) Schiff Base Complex with Dioxygen. *Inorg. Chem.* **1998**, *37*, 2134–2140.

(27) (a) Gagnon, N.; Tolman, W. B. $[\text{CuO}]^+$ and $[\text{CuOH}]^{2+}$ Complexes: Intermediates in Oxidation Catalysis? *Acc. Chem. Res.* **2015**, *48*, 2126–2131. (b) Dhar, D.; Yee, G. M.; Markle, T. F.; Mayer, J. M.; Tolman, W. B. Reactivity of the Copper(III)-Hydroxide unit with Phenols. *Chem. Sci.* **2017**, *8*, 1075–1085.

(28) Conde, A.; Mar Díaz-Requejo, M.; Perez, P. J. Direct, Copper-Catalyzed Oxidation of Aromatic C-H Bonds with Hydrogen Peroxide under Acid-free Conditions. *Chem. Commun.* **2011**, *47*, 8154–8156.

(29) Vilella, L.; Conde, A.; Balcells, D.; Diaz-Requejo, M. M.; Lledos, A.; Perez, P. J. A Competing, Dual Mechanism for Catalytic Direct Benzene Hydroxylation from Combined Experimental-DFT Studies. *Chem. Sci.* **2017**, *8*, 8373–8383.

(30) Tsuji, T.; Zaoputra, A. A.; Hitomi, Y.; Mieda, K.; Ogura, T.; Shiota, Y.; Yoshizawa, K.; Sato, H.; Kodera, M. Specific Enhancement of Catalytic Activity by a Dicopper Core: Selective Hydroxylation of Benzene to Phenol with Hydrogen Peroxide. *Angew. Chem., Int. Ed.* **2017**, *56*, 7779–7782.

(31) Xu, B.; Zhong, W.; Wei, Z.; Wang, H.; Liu, J.; Wu, L.; Feng, Y.; Liu, X. Synthesis and Characterization of Copper(II) Complexes with Multidentate Ligands as Catalysts for the Direct Hydroxylation of Benzene to Phenol. *Dalton Trans.* **2014**, *43*, 15337–15345.

(32) Mayilmurugan, R.; Stoeckli-Evans, H.; Palaniandavar, M. Novel Iron(III) Complexes of Sterically Hindered 4N Ligands: Regioselectivity in Biomimetic Extradiol Cleavage of Catechols. *Inorg. Chem.* **2008**, *47*, 6645–6658.

(33) (a) Dhanalakshmi, T.; Suresh, E.; Stoeckli-Evans, H.; Palaniandavar, M. New Copper(II) Complexes as Efficient Catalysts for Olefin Aziridination: The Effect of Ligand Steric Hindrance on Re-activity. *Eur. J. Inorg. Chem.* **2006**, *2006*, 4687–4695. (b) Kim, S.; Ginsbach, J. W.; Billah, A. I.; Siegler, M. A.; Moore, C. D.; Solomon, E. I.; Karlin, K. D. Tuning of the Copper–Thioether Bond in Tetradentate N_3S (thioether) Ligands; O–O Bond Reductive Cleavage via a $[\text{Cu}^{\text{II}}(\mu\text{-}1,2\text{-peroxo})]^{2+}/[\text{Cu}^{\text{III}}(\mu\text{-}oxo)_2]^{2+}$ Equilibrium. *J. Am. Chem. Soc.* **2014**, *136*, 8063–8071.

(34) Schmidt, M.; Wiedemann, D.; Moubaraki, B.; Chilton, N. F.; Murray, K. S.; Vignesh, K. R.; Rajaraman, G.; Grohmann, A. Iron(II) Complexes of Two Amine/Imine N_5 Chelate Ligands Containing a 1,4-Diazepane Core - To Crossover or Not to Crossover. *Eur. J. Inorg. Chem.* **2013**, *5–6*, 958–967.

(35) Muthuramalingam, S.; Subramanian, S.; Khamrang, T.; Velusamy, M.; Mayilmurugan, R. Copper(II)-Bioinspired Models for Copper Amine Oxidases: Oxidative Half-Reaction in Water. *ChemistrySelect* **2017**, *2*, 940–948.

(36) Addison, A. W.; Rao, T. N.; Reedijk, J.; van Rijn, J.; Verschoor, G. C. Synthesis, Structure, and Spectroscopic Properties of Copper(II) Compounds Containing Nitrogen–Sulphur Donor Ligands; the Crystal and Molecular Structure of Aqua[1,7-bis(N-methylbenzimidazol-2'-yl)-2,6-dithiaheptane]copper(II) perchlorate. *J. Chem. Soc., Dalton Trans.* **1984**, *7*, 1349–1356.

(37) Yao, Y.; Perkovic, M. W.; Rillemo, D. P.; Woods, C. Structures and Properties of Copper(II) and Copper(I) Complexes Containing an Ethane-bridged Dimeric Phenanthroline Ligand. *Inorg. Chem.* **1992**, *31*, 3956–3962.

(38) Lever, A. B. P. *Inorganic Electronic Spectroscopy*, 2nd ed.; Elsevier: Amsterdam, The Netherlands, 1984.

(39) (a) Amundsen, A. R.; Whelan, J.; Bosnich, B. Biological Analogs. Nature of the Binding Sites of Copper-Containing Proteins. *J. Am. Chem. Soc.* **1977**, *99*, 6730–6739. (b) Ettinger, M. J. Spectral Properties of “non-blue” Cupric Copper in Proteins. Circular Dichroism and Optical Spectra of Galactose Oxidase. *Biochemistry* **1974**, *13*, 1242–1247.

(40) Uma, R.; Viswanathan, R.; Palaniandavar, M.; Lakshminarayanan, M. Copper(II) Complexes of Novel Tripodal Ligands Containing Phenolate and Benzimidazole/Pyridine Pendants: Synthesis, Structure, Spectra and Electrochemical Behaviour. *J. Chem. Soc., Dalton Trans.* **1994**, *8*, 1219–1226.

(41) (a) Cai, D.; Klinman, J. P. Copper Amine Oxidase: Heterologous Expression, Purification, and Characterization of An Active Enzyme in *Saccharomyces cerevisiae*. *Biochemistry* **1994**, *33*, 7647–7653. (b) Rajarajeswari, C.; Loganathan, R.; Palaniandavar, M.; Suresh, E.; Riyasdeen, A.; Akbarsha, M. A. Copper(II) Complexes with 2NO and 3N Donor Ligands: Synthesis, Structures, and Chemical Nuclease and Anticancer Activities. *Dalton Trans.* **2013**, *42*, 8347–8363.

(42) (a) Dittler-Klingemann, A. M.; Orvig, C.; Hahn, F. E.; Thaler, F.; Hubbard, C. D.; van Eldik, R.; Schindler, S.; Fabian, I. Geometric Factors in the Structural and Thermodynamic Properties of Copper(II) Complexes with Tripodal Tetraamines. *Inorg. Chem.* **1996**, *35*, 7798–7803. (b) Solomon, E. I.; Heppner, D. E.; Johnston, E. M.; Ginsbach, J. W.; Cirera, J.; Qayyum, M.; Kieber-Emmons, M. T.; Kjaergaard, C. H.; Hadt, R. G.; Tian, L. Copper Active Sites in Biology. *Chem. Rev.* **2014**, *114*, 3659–3853.

(43) (a) Solomon, E. I.; Szilagy, R. K.; DeBeer George, S.; Basumallick, L. Electronic Structures of Metal Sites in Proteins and Models: Contributions to Function in Blue Copper Proteins. *Chem. Rev.* **2004**, *104*, 419–458. (b) Solomon, E. I. Dioxygen Binding, Activation, and Reduction to H_2O by Cu Enzymes. *Inorg. Chem.* **2016**, *55*, 6364–6375. (c) Kjaergaard, C. H.; Jones, S. M.; Gounel, S.; Mano, N.; Solomon, E. I. Two-Electron Reduction versus One-Electron Oxidation of the Type 3 Pair in the Multicopper Oxidases. *J. Am. Chem. Soc.* **2015**, *137*, 8783–8794.

(44) (a) Hathaway, B. J.; Tomlinson, A. A. G. Copper(II) ammonia complexes. *Coord. Chem. Rev.* **1970**, *5*, 1–43. (b) Hathaway, B. J. In *Comprehensive Coordination Chemistry*; Wilkinson, G., Gillard, R. D., McCleverty, J. A., Eds.; Pergamon Press: Oxford, England, 1987; Vol. 5, p 533. (c) Addison, A. W. Copper Coordination Chemistry. In *Biochemical and Inorganic Perspectives*; Karlin, K. D., Zubieta, J., Eds.; Adenine: Guilderland, NY, 1983; p 109. (d) Sakaguchi, U.; Addison, A. W. Spectroscopic and Redox Studies of some Copper(II) Complexes with Biomimetic Donor Atoms: Implications for Protein Copper Centres. *J. Chem. Soc., Dalton Trans.* **1979**, *4*, 600–608.

(45) (a) Garribba, E.; Micera, G. The Determination of the Geometry of Cu(II) Complexes. *J. Chem. Educ.* **2006**, *83*, 1229. (b) Laurie, S. H.; Lund, T.; Raynor, J. B. Electronic Absorption and Electron Spin Resonance Studies on the Interaction between the Biologically Relevant Copper(II) Glycylglycine and L-Histidine Complexes with D-Penicillamine. *J. Chem. Soc., Dalton Trans.* **1975**, *1389–1394*.

(46) (a) Muthuramalingam, S.; Khamrang, T.; Velusamy, M.; Mayilmurugan, R. Mayilmurugan, Catalytic Fixation of Atmospheric Carbon Dioxide by Copper(II) Complexes of Bidentate Ligands. *Dalton Trans.* **2017**, *46*, 16065–16076. (b) Kooter, I. M.; Steiner, R. A.; Dijkstra, B. W.; Van Noort, P. I.; Egmond, M. R.; Huber, M. EPR Characterization of the Mononuclear Cu-containing *Aspergillus Japonicus* Quercetin 2,3-dioxygenase Reveals Dramatic Changes Upon Anaerobic Binding of Substrates. *Eur. J. Biochem.* **2002**, *269*, 2971–2979. (c) Muthuramalingam, S.; Maheshwaran, D.; Velusamy, M.; Mayilmurugan, R. Regioselective Oxidative Carbon-Oxygen Bond Cleavage Catalysed by Copper(II) Complexes: A Relevant Model Study for Lytic Polysaccharides Monooxygenases Activity. *J. Catal.* **2019**, *372*, 352–361.

(47) (a) Solomon, E. I. Spectroscopic Methods in Bioinorganic Chemistry: Blue to Green to Red Copper Sites. *Inorg. Chem.* **2006**, *45*, 8012–8025. (b) Rapheal, P. F.; Manoj, E.; Prathapachandra Kurup,

M. R. Copper(II) Complexes of N(4)-substituted Thiosemicarbazones derived from Pyridine-2-carbaldehyde: Crystal Structure of a Binuclear Complex. *Polyhedron* **2007**, *26*, 818–828. (c) Sohtun, W. P.; Muthuramalingam, S.; Velusamy, M.; Mayilmurugan, R. Mayilmurugan, New Class of Tridentate 3N Ligands and Copper(II) Complexes: A Model for Type-2 Copper Site of Phenoxazinone Synthase. *Inorg. Chem. Commun.* **2019**, *110*, 107608.

(48) (a) Schatz, M.; Leibold, M.; Foxon, S. P.; Weitzer, M.; Heinemann, F. W.; Hampel, F.; Walter, O.; Schindler, S. Syntheses and Characterization of Copper Complexes of the Ligand (2-aminoethyl)bis(2-pyridylmethyl)amine (uns-penp) and derivatives. *Dalton Trans.* **2003**, *8*, 1480–1487. (b) Weitzer, M.; Schatz, M.; Hampel, F.; Heinemann, F. W.; Schindler, S. Low-Temperature Stopped-flow Studies in Inorganic Chemistry. *J. Chem. Soc., Dalton Trans.* **2002**, *24*, 686–694.

(49) (a) Poater, A.; Ragone, F.; Mariz, R.; Dorta, R.; Cavallo, L. Comparing the Enantioselective Power of Steric and Electrostatic Effects in Transition-Metal-Catalyzed Asymmetric Synthesis. *Chem. - Eur. J.* **2010**, *16*, 14348–14353. (b) Falivene, L.; Cao, Z.; Petta, A.; Serra, L.; Poater, A.; Oliva, R.; Scarano, V.; Cavallo, L. Towards the Online Computer-Aided Design of Catalytic Pockets. *Nat. Chem.* **2019**, *11*, 872–879. (c) Poater, A.; Cosenza, B.; Correa, A.; Giudice, S.; Ragone, F.; Scarano, V.; Cavallo, L. Samb Vca: A Web Application for the Calculation of the Buried Volume of N-Heterocyclic Carbene Ligands. *Eur. J. Inorg. Chem.* **2009**, *2009*, 1759–1766.

(50) Luo, Y. R. *Comprehensive Handbook of Chemical Bond Energies*; CRC Press: Boca Raton, FL, 2007.

(51) (a) Holland, P. L.; Rodgers, K. R.; Tolman, W. B. Is the Bis(μ -oxo)dicopper Core Capable of Hydroxylating an Arene? *Angew. Chem., Int. Ed.* **1999**, *38*, 1139–1142. (b) Honda, K.; Cho, J.; Matsumoto, T.; Roh, J.; Furutachi, H.; Tosha, T.; Kubo, M.; Fujinami, S.; Ogura, T.; Kitagawa, T.; Suzuki, M. Oxidation Reactivity of Bis(μ -oxo) Dinickel(III) Complexes: Arene Hydroxylation of the Supporting Ligand. *Angew. Chem., Int. Ed.* **2009**, *48*, 3304–3307.

(52) Augusti, R.; Dias, A. O.; Rocha, L. L.; Lago, R. M. Kinetics and Mechanism of Benzene Derivative Degradation with Fenton's Reagent in Aqueous Medium Studied by MIMS. *J. Phys. Chem. A* **1998**, *102*, 10723–10727.

(53) Emmert, M. H.; Cook, A. K.; Xie, Y. J.; Sanford, M. S. Remarkably High Reactivity of Pd(OAc)₂/Pyridine Catalysts: Non-directed C-H Oxygenation of Arenes. *Angew. Chem., Int. Ed.* **2011**, *50*, 9409–9412.

(54) Ohkubo, K.; Kobayashi, T.; Fukuzumi, S. Direct Oxygenation of Benzene to Phenol Using Quinolinium Ions as Homogeneous Photocatalysts. *Angew. Chem., Int. Ed.* **2011**, *50*, 8652–8655.

(55) (a) Balula, M. S.; Gamelas, J. A.; Carapuça, H. M.; Cavaleiro, A. M. V.; Schlindwein, W. Electrochemical Behaviour of First Row Transition Metal Substituted Polyoxotungstates: A Comparative Study in Acetonitrile. *Eur. J. Inorg. Chem.* **2004**, *2004*, 619–628. (b) Thorp, H. H. *Encyclopedia of Inorganic and Bioinorganic Chemistry*; John Wiley & Sons, Ltd., 2011. (c) Lemoine, P. Electrochemistry of transition metal clusters. *Coord. Chem. Rev.* **1982**, *47*, 55–88.

(56) (a) Kundu, S.; Matito, E.; Walleck, S.; Pfaff, F. F.; Heims, F.; Rabay, B.; Luis, J. M.; Company, A.; Braun, B.; Glaser, T.; Ray, K. O-O Bond Formation Mediated by a Hexanuclear Iron Complex Supported on a Stannoxane Core. *Chem. - Eur. J.* **2012**, *18*, 2787–2791. (b) Parham, J. D.; Wijeratne, G. B.; Rice, D. B.; Jackson, T. A. Spectroscopic and Structural Characterization of Mn(III)-Alkylperoxo Complexes Supported by Pentadentate Amide-Containing Ligands. *Inorg. Chem.* **2018**, *57*, 2489–2502. (c) Reynolds, M. S.; Butler, A. Oxygen-17 NMR, Electronic, and Vibrational Spectroscopy of Transition Metal Peroxo Complexes: Correlation with Reactivity. *Inorg. Chem.* **1996**, *35*, 2378–2383. (d) Coggins, M. K.; Kovacs, J. A. Structural and Spectroscopic Characterization of Metastable Thiolate-Ligated Manganese(III)-Alkylperoxo Species. *J. Am. Chem. Soc.* **2011**, *133*, 12470–12473. (e) Coggins, M. K.; Martin-Diaconescu, V.; DeBeer, S.; Kovacs, J. A. Correlation Between Structural, Spectroscopic, and Reactivity Properties Within a Series of Structurally

Analogous Metastable Manganese(III)-Alkylperoxo Complexes. *J. Am. Chem. Soc.* **2013**, *135*, 4260–4272.

(57) Peterson, R. L.; Himes, R. A.; Kotani, H.; Suenobu, T.; Tian, L.; Siegler, M. A.; Solomon, E. I.; Fukuzumi, S.; Karlin, K. D. Cupric Superoxo-Mediated Intermolecular C-H Activation Chemistry. *J. Am. Chem. Soc.* **2011**, *133*, 1702–1705.

(58) Xing, Q.; Lv, H.; Xia, C.; Li, F. Iron-catalyzed Aerobic Oxidative Cleavage of the C–C σ -bond using Air as the Oxidant: Chemoselective Synthesis of Carbon Chain-shortened Aldehydes, Ketones, and 1,2-dicarbonyl Compounds. *Chem. Commun.* **2016**, *52*, 489–492.

(59) (a) Prat, I.; Mathieson, J. S.; Güell, M.; Ribas, X.; Luis, J. M.; Cronin, L.; Costas, M. Observation of Fe(V)=O Using Variable-Temperature Mass Spectrometry and its Enzyme-like C–H and C=C Oxidation Reactions. *Nat. Chem.* **2011**, *3*, 788–793. (b) Garcia-Bosch, I.; Siegler, M. A. Copper-Catalyzed Oxidation of Alkanes with H₂O₂ under a Fenton-like Regime. *Angew. Chem., Int. Ed.* **2016**, *55*, 12873–12876. (c) Gómez, L.; Garcia-Bosch, I.; Company, A.; Benet-Buchholz, J.; Polo, A.; Sala, X.; Ribas, X.; Costas, M. Stereospecific C-H Oxidation with H₂O₂ Catalyzed by a Chemically Robust Site-Isolated Iron Catalyst. *Angew. Chem., Int. Ed.* **2009**, *48*, 5720–5723.

(60) Cho, K.-B.; Wu, X.; Lee, Y.-M.; Kwon, Y.-H.; Shaik, S.; Nam, W. Evidence for an Alternative to the Oxygen Rebound Mechanism in C-H Bond Activation by Non-Heme Fe^{IV}O Complexes. *J. Am. Chem. Soc.* **2012**, *134*, 20222–20225.

(61) (a) Schaefer, A.; Horn, H.; Ahlrichs, R. Fully Optimized Contracted Gaussian Basis Sets for Atoms Li to Kr. *J. Chem. Phys.* **1992**, *97*, 2571–2577. (b) Weigend, F.; Ahlrichs, R. Balanced Basis Sets of Split Valence, Triple Zeta Valence and Quadruple Zeta Valence Quality for H to Rn: Design and Assessment of Accuracy. *Phys. Chem. Chem. Phys.* **2005**, *7*, 3297–3305.

(62) Wada, A.; Harata, M.; Hasegawa, K.; Jitsukawa, K.; Masuda, H.; Mukai, M.; Kitagawa, T.; Einaga, H. Structural and Spectroscopic Characterization of a Mononuclear Hydroperoxo-Copper(II) Complex with Tripodal Pyridylamine Ligands. *Angew. Chem., Int. Ed.* **1998**, *37*, 798–799.

(63) Kim, B.; Jeong, D.; Ohta, T.; Cho, J. Nucleophilic Reactivity of a Copper(II)-Hydroperoxo Complex. *Commun. Chem.* **2019**, *2*, 1–6.

(64) (a) Ansari, A.; Jayapal, P.; Rajaraman, G. C-H Bond Activation by Metal-Superoxo Species: What Drives High Reactivity? *Angew. Chem., Int. Ed.* **2014**, *54*, 564–568. (b) Oh, H.; Ching, W.-M.; Kim, J.; Lee, W.-Z.; Hong, S. Hydrogen Bond-Enabled Heterolytic and Homolytic Peroxide Activation within Nonheme Copper(II)-Alkylperoxo Complexes. *Inorg. Chem.* **2019**, *58* (19), 12964–12974. (c) Neisen, B. D.; Gagnon, N. L.; Dhar, D.; Spaeth, A. D.; Tolman, W. B. Formally Copper(III)-Alkylperoxo Complexes as Models of Possible Intermediates in Monooxygenase Enzymes. *J. Am. Chem. Soc.* **2017**, *139*, 10220–10223.

(65) Frisch, M. J.; Trucks, G. W.; Schlegel, H. B.; Scuseria, G. E.; Robb, M. A.; Cheeseman, J. R.; Scalmani, G.; Barone, V.; Mennucci, B.; Petersson, G. A.; Nakatsuji, H.; Caricato, M.; Li, X.; Hratchian, H. P.; Izmaylov, A. F.; Bloino, J.; Zheng, G.; Sonnenberg, J. L.; Hada, M.; Ehara, M.; Toyota, K.; Fukuda, R.; Hasegawa, J.; Ishida, M.; Nakajima, T.; Honda, Y.; Kitao, O.; Nakai, H.; Vreven, T.; Montgomery, J. A., Jr.; Peralta, J. E.; Ogliaro, F.; Bearpark, M. J.; Heyd, J.; Brothers, E. N.; Kudin, K. N.; Staroverov, V. N.; Kobayashi, R.; Normand, J.; Raghavachari, K.; Rendell, A. P.; Burant, J. C.; Iyengar, S. S.; Tomasi, J.; Cossi, M.; Rega, N.; Millam, N. J.; Klene, M.; Knox, J. E.; Cross, J. B.; Bakken, V.; Adamo, C.; Jaramillo, J.; Gomperts, R.; Stratmann, R. E.; Yazyev, O.; Austin, A. J.; Cammi, R.; Pomelli, C.; Ochterski, J. W.; Martin, R. L.; Morokuma, K.; Zakrzewski, V. G.; Voth, G. A.; Salvador, P.; Dannenberg, J. J.; Dapprich, S.; Daniels, A. D.; Farkas, O.; Foresman, J. B.; Ortiz, J. V.; Cioslowski, J.; Fox, D. J. *Gaussian 09*; Gaussian Inc.: Dordrecht, The Netherlands, 2009.